Thermoelectric and memristive features of the $Sb_2Te_3/Sb_2S_3/Sb_2Te_3$ and $Ag/Sb_2Te_3/Ag$ structures

© A. Papikyan[2], S. Harutyunyan[1,2], N. Aghamalyan[1,2], R. Hovsepyan[1,2], A. Khachaturova[1], S. Petrosyan[1,2], G. Badalyan[1], E. Kafadaryan[1,2]

[1] Institute for Physical Research, National Academy of Sciences of Armenia, 0203 Ashtarak-2, Armenia
[2] Russian-Armenian University, 0051 Yerevan, Armenia

E-mail: ekafadaryan@gmail.com

Received November 11, 2021
Revised November 16, 2021
Accepted November 16, 2021

Single-layer Sb_2Te_3 films and three-layer $Sb_2Te_3/Sb_2S_3/Sb_2Te_3$ structures are obtained by thermal vacuum deposition. Their thermoelectric characteristics have been investigated in a wide temperature range (5−350 K). It is shown that the conductivity of $Sb_2Te_3/Sb_2S_3/Sb_2Te_3$ has a semiconductor behavior, the resistivity is an order of magnitude higher than the resistivity of the Sb_2Te_3 film; the Seebeck coefficient of $Sb_2Te_3/Sb_2S_3/Sb_2Te_3$ is 1.5 and 3 times higher than the Seebeck coefficient of the film and single-crystal Sb_2Te_3, respectively. The current–voltage characteristics of the Sb_2Te_3 film exhibit memristive properties with unipolar resistive switching, whereas $Sb_2Te_3/Sb_2S_3/Sb_2Te_3$ can be considered as a memristor with a parallel connected capacitance.

Keywords: Sb_2S_3, Sb_2Te_3, films, volt-ampere characteristic, Seebeck coefficient, memristor.

DOI: 10.21883/SC.2022.03.53071.9770

1. Introduction

The investigation of thermoelectrical and memristive properties of chalcogenide-based structures (A^V-B^{VI} compounds) is of interest due to two emerging applications such as domain and phonon engineering that uses multilayer structures to enable production of both thermoelements with very low thermal conductivity [1–3] and memristors [4–6] constituting resistive random-access memory (RRAM) that can expand the research area and offer opportunities of application as biological synapse equivalents [7], biocomputation systems [8] and neural networks [9]. Combination of memristance and thermoelectricity in a single device ensures multifunctional capabilities of the chalcogenide-based devices. The promising materials for production of non-volatile storage thermoelectric cells may include film systems on the basis of antimony telluride (Sb_2Te_3) and antimony sulphide (Sb_2S_3). In particular, combination of these compounds, without trying to find the best chemical composition, may improve the characteristics of the devices produced on their basis.

Scientific literature describes a wide range of experimental research for investigation of both thermoelectrical [1–3] and memristive [4–6] properties of semiconductor Sb_2Te_3 and Sb_2S_3 that have high Seebeck coefficient and Q factor. However, there are no publications addressing thermoelectrical and memristive properties together.

In view of the foregoing, the purpose of the research was to produce Sb_2Te_3 films and three-layer $Sb_2Te_3/Sb_2S_3/Sb_2Te_3$ structure and investigate their thermoelectrical and memristive properties.

2. Experimental procedure

Three-layer $Sb_2Te_3/Sb_2S_3/Sb_2Te_3$ structure composed of Sb_2S_3 layer sandwiched between Sb_2Te_3 electrodes was produced on a glass substrate by thermal vacuum evaporation at room temperature with 100/100/150 nm film thicknesses, respectively, and then annealed in nitrogen atmosphere at 180°C during 5 h. A 42 nm Sb_2Te_3 film was also evaporated on a glass substrate with a 100 nm silver coating and annealed in nitrogen atmosphere at 180°C during 5 h. Top electrode (Ag) thickness was 100 nm. The area of Sb_2Te_3 and Ag top electrodes was 0.342 mm^2. Phase composition of the films was examined using Panalytical Empyrean X-ray diffractometer using Bragg−Brentano geometry with emission CuK_α ($\lambda = 1.5418$ Å). Surface morphology and element composition of the samples were examined using a scanning election microscope (SEM VEGA TS-5130MM) with INCA Energy 300 X-ray energy dispersive spectroscopy (EDS) system.

Resistivity of the samples in the range of 5−350 K was measured by a four-contact method in horizontal configuration along the film length. The extreme contacts served for current readings and the middle contacts served for voltage readings. Thermopower, S, was measured along the film length. Two contacts were used. The temperature difference was achieved by attachment of a miniature ohmic heater near one of the contacts where temperature T_1 was reached, with other contact remaining at background temperature T_0. Thermopower in the same temperature range was calculated as $S = \Delta U/\Delta T$ ($\Delta T = T_1 - T_0$, $\Delta U = U_1 - U_0$), where U_1 and U_0 are voltages at T_1 and T_0, respectively, measured using Keithley 181 and Keithley 2182A nanovoltmeters.

The sample was kept at a homogeneous temperature using Scientific Instruments 9650 digital temperature controller. Measurements were performed in Cryomech ST405 cryostat.

Current-voltage characteristics $(I-V)$ in vertical configuration were measured at room temperature, 30 mHz and bias voltage from -10.0 to $+10.0$ V using Agilent 33500B digital waveform generator and UNI-T UT61C digital multimeters.

3. Experimental results

Figure 1 shows X-ray images of Sb_2S_3/Sb_2Te_3, Sb_2Te_3/Ag and single-crystal Sb_2Te_3 structures. Diffraction halos on the X-ray images suggest that the structures are composed of amorphous chalcogenide films. Diffraction halo with a maximum between 20 and 30° is observed on X-ray images of both Sb_2S_3/Sb_2Te_3 (Fig. 1, *a*) and Sb_2Te_3/Ag (Fig. 1, *b*) structures and can be caused by both glass-like Sb_2Te_3, and Sb_2S_3, because this band corresponds to one of the most intensive peaks observed in crystalline Sb_2Te_3 and Sb_2S_3 [10,11]. The band near $2\theta = 40°$ may be assigned to Sb_2S_3 [11]. These findings agree with [12] which states that wide maxima in many chalcogenide glasses are located in positions where intense diffraction peaks are present in crystalline homologs. Peaks $2\theta = 38.3402$, 44.4941, 64.6579, 77.6917, 81.7135° in Fig. 1, *b* are caused by Ag that serves as a bottom contact in $Ag/Sb_2Te_3/Ag$ structure. Sb_2Te_3 and Sb_2S_3 micrographs in Fig. 2 show that the film surfaces are smooth and homogenous. For a single-layer Sb_2Te_3 film, concentration ratio Sb : Te = 39.62 : 60.38 at% was obtained and for a three-layer structure in Sb_2S_3 layer, ratio S : Sb = 40.39 : 59.61 at% was obtained.

Figure 3 shows resistivity-temperature dependences $\rho(T)$ of $Sb_2Te_3/Sb_2S_3/Sb_2Te_3$, $Ag/Sb_2Te_3/Ag$ and single-crystal Sb_2Te_3 structures. The single crystal demonstrates semimetallic behavior throughout the temperature range which agrees with [10–12]. By contrast, thin amorphous Sb_2Te_3 film demonstrates semiconductor behavior from 3 to 250 K and semimetallic behavior at higher temperatures. Such behavior may be explained by inadequate annealing time and temperature resulting in formation of an amorphous structure displayed on the X-ray images. Three-layer $Sb_2Te_3/Sb_2S_3/Sb_2Te_3$ structure demonstrates semiconductor behavior throughout the temperature range, where resistance at room temperature is, respectively, 3 and 37.5 times greater than that of Sb_2Te_3 amorphous film and single crystal; this difference increases with a decrease in temperature. Figure 4 shows Seebeck coefficient-temperature dependences $S(T)$ of the test samples. The samples have positive Seebeck coefficient, i.e. *p*-type conductivity, which agrees with [13]. Seebeck coefficient increases with the temperature, whereby Sb_2Te_3 single crystal has the lowest S, which may be explained by anisotropy and measurement of S in crystal plane $a-b$ with high conductivity. Seebeck

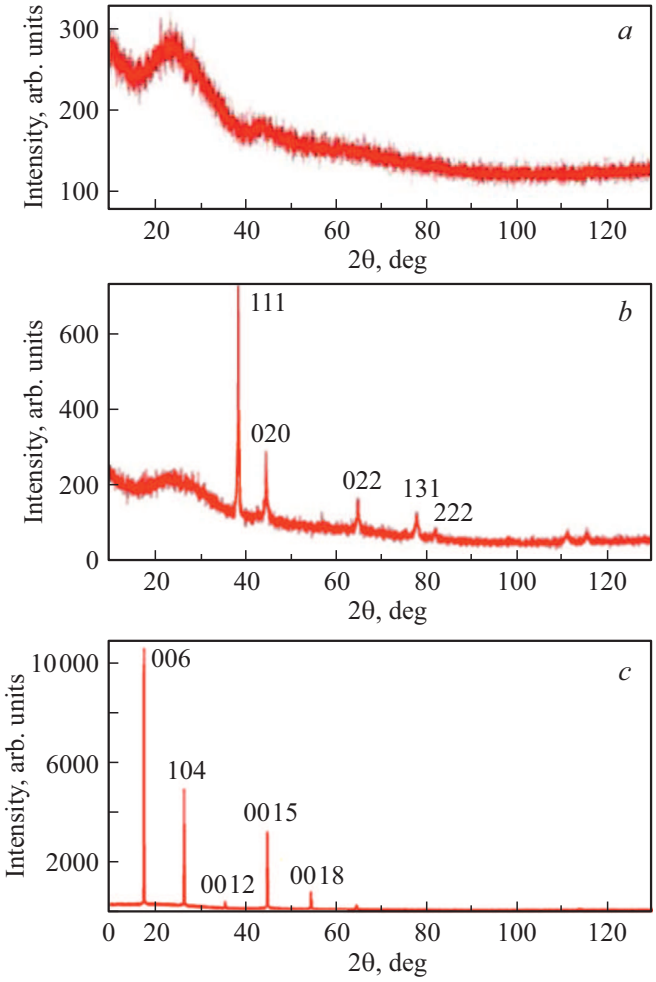

Figure 1. X-ray images of Sb_2S_3/Sb_2Te_3 (*a*), Sb_2Te_3/Ag (*b*) structures and Sb_2Te_3 single crystal (*c*).

coefficient of three-layer $Sb_2Te_3/Sb_2S_3/Sb_2Te_3$ structure is 1.5 and 3 times greater than that of the amorphous and crystalline Sb_2Te_3, respectively. We suppose that the presence of sulfur that has a higher electronegativity than tellurium reduces the hole concentration which leads to an increase in Seebeck coefficient. In case of degenerate semiconductors, Seebeck coefficient S is defined by Mott ratio [14]

$$S = (8\pi^2 k^2 T/3eh^2) m_d^* (\pi/3n)^{2/3}, \quad (1)$$

where k is Boltzmann constant, m_d^* is the effective carrier mass, e is the electron charge, h is Planck's constant and T is the measurement temperature. Equation (1) shows that S is linearly dependent on the temperature for degenerate semiconductors. Temperature dependence S of the single crystal is almost linear, i.e. the single crystal is supposed to be a degenerate semiconductor. On temperature dependences S of structures (Fig. 4, *b* and *c*), there is a delinearity and a „step" feature specific to disordered systems is observed at 170 K for single-layer Sb_2Te_3 film and at 102 and 270 K for three-layer $Sb_2Te_3/Sb_2S_3/Sb_2Te_3$ structure. With further

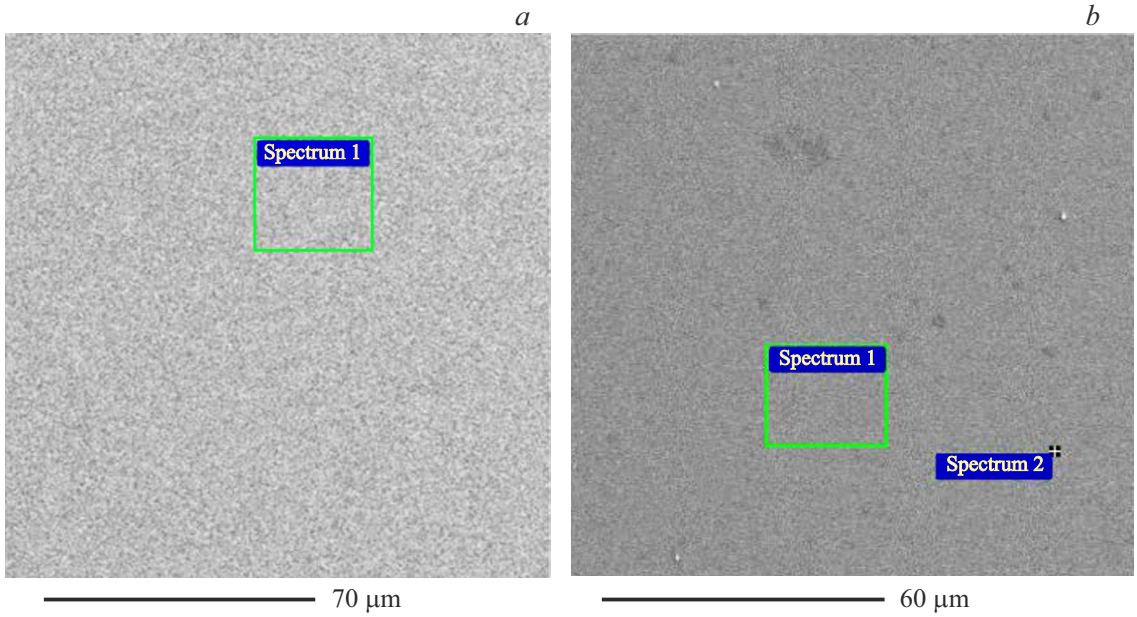

Figure 2. Micrographs of Sb_2Te_3 (a) and Sb_2S_3 (b) surfaces.

increase in temperature, Seebeck coefficient increases, but with other slope. The origin of the specific „knee" of curve $S(T)$ means that Mott's equation is not fulfilled. It is widely believed that this feature is a result of electron-phonon interaction effect which renormalizes the electron energy and relaxation time [15,16]. In addition, the linear behavior of thermopower was discussed on the basis of the temperature dependence of electron structure factor and nonelastic electron-electron interaction [16].

Figure 5 shows the samples' thermoelectric power (TEP)-temperature dependences $P(T) = S^2/\rho$. The data was calculated according to the measurements of $S(T)$ and $\rho(T)$.

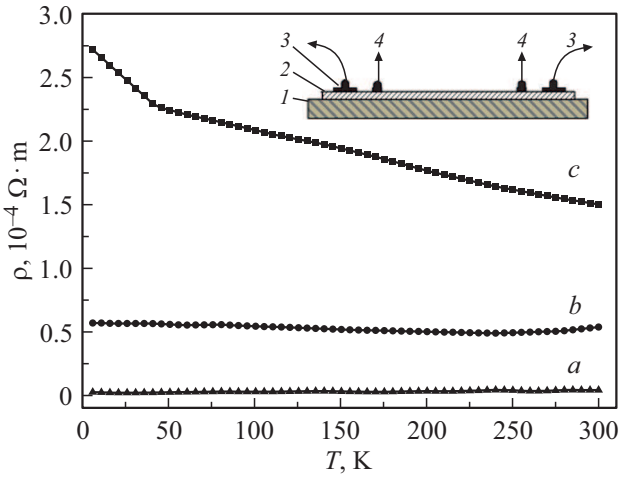

Figure 3. The resistivity-temperature dependences of Sb_2Te_3 (a) single crystal, Sb_2Te_3 (b) film and $Sb_2Te_3/Sb_2S_3/Sb_2Te_3$ (c) structure. Detail — sample diagram, *1* — substrate, *2* — Sb_2Te_3 film or $Sb_2Te_3/Sb_2S_3/Sb_2Te_3$ structure to be measured, *3* and *4* — silver contacts for current and voltage measurement, respectively.

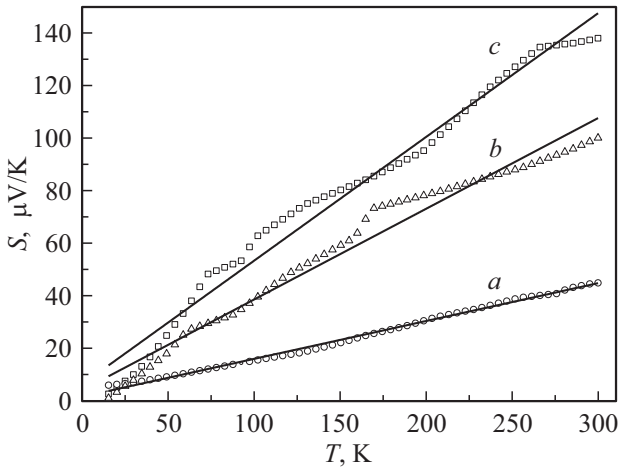

Figure 4. The Seebeck coefficient-temperature dependences of Sb_2Te_3 (a) single crystal, Sb_2Te_3 (b) film and $Sb_2Te_3/Sb_2S_3/Sb_2Te_3$ (c) structure.

High TEP coefficient is observed in the single crystal at room temperature probably due to high single crystal conductivity.

Figure 6 shows volt-ampere characteristic curve $(I-V)$ of $Ag/Sb_2Te_3/Ag$ structure measured at room temperature. As shown in Fig. 6, $Ag/Sb_2Te_3/Ag$ structure has unipolar resistive switching in the range from -700 to $+700$ mV, where the device may be switched on and off at the same voltage polarity with ratio $R_{off}/R_{sw} \sim 200$. $Ag/Sb_2Te_3/Ag$ device is switched into low-resistive condition (LRS) at $V = 690$ mV. With an increase in the number of cycles, the switching threshold of memristor is displaced into the lower voltage area of 580–690 mV. Thermal effect that

occurs when current flows through the sample can create a conductivity path that moves the device into „on" state. Sb_2Te_3, being a binary chemical compound, is characterized by a strong dependence of the material resistance vs. phase state [17,18]. As shown in Fig. 3, temperature resistance of amorphous Sb_2Te_3 at room temperature is one order of magnitude greater than that of a crystalline compound, and in this case the path conductivity changes as a result of its transition from amorphous into crystalline phase. Transition from amorphous into crystalline state takes place in the 700 mV region (Fig. 6). At such voltages, current flowing through the path achieves 6 A, which is sufficient for transition into low resistance state. For reverse transition into the high resistance state, a current pulse is applied with a higher amplitude sufficient to achieve the melting point. Chalcogenide goes into the high resistance state during several nanoseconds [19].

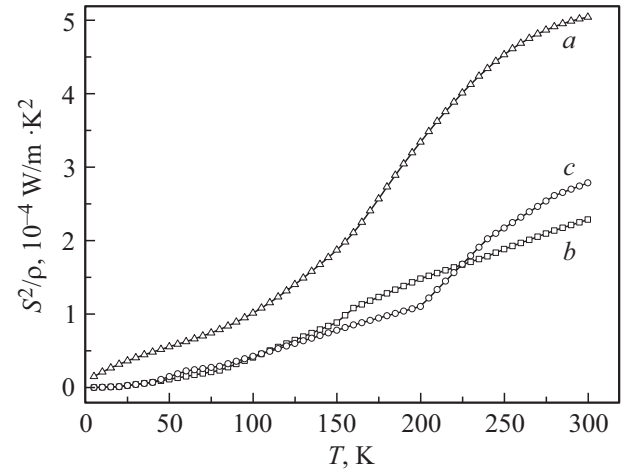

Figure 5. The thermoelectric power-temperature dependences of Sb_2Te_3 (*a*) single crystal, Sb_2Te_3 (*b*) film and $Sb_2Te_3/Sb_2S_3/Sb_2Te_3$ (*c*) structure.

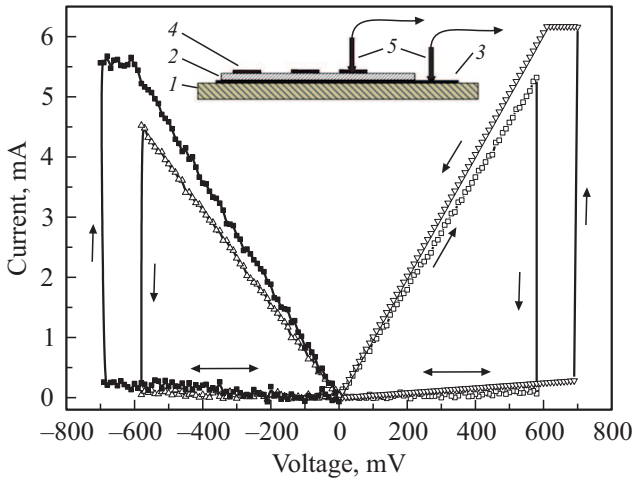

Figure 6. CVC of $Ag/Sb_2Te_3/Ag$ structure. In detail — sample diagram: *1* — substrate, *2* — Sb_2Te_3 film, *3* and *4* — silver contacts, *5* — current and voltage probes.

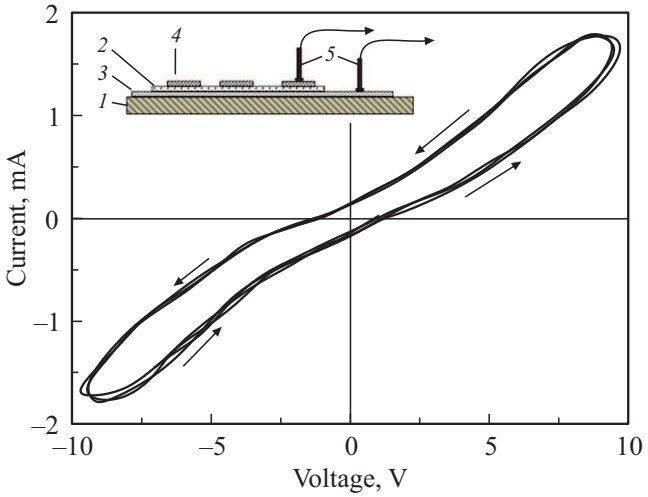

Figure 7. CVC of $Sb_2Te_3/Sb_2S_3/Sb_2Te_3$ structure. In detail — sample diagram: *1* — substrate, *2* — Sb_2S_3 film, *3, 4* — Sb_2Te_3 contacts, *5* — current and voltage probes.

Figure 7 shows $I-V$ curve of $Sb_2Te_3/Sb_2S_3/Sb_2Te_3$ structure measured at 30 mHz; *I-V* curve is nonlinear and hysteresis loop exhibits nonezero-crossing $I-V$ characteristic (non-zero intersection). When the external voltage decreases to zero, internal electric field induced by capacitance is non-zero ($I_+ = 0.14$ mA, $I_- = -0.16$ mA; $V_+ = 1.1$ V, $V_- = -1.37$ V). In other words, residual current is present and hysteresis curve $I-V$ may be treated as linear addition of capacitor and memristor currents. In terms of circuit equivalent, a similar $I-V$ curve may be obtained when the capacitance and memristor are connected in parallel, which agrees with [20,21], where eight types of specific non-zero axial non-linear $I-V$ curve are calculated. Hysteresis loop in Fig. 7 corresponds to the theoretically calculated $I-V$ curve provided in [20,21] and is composed of capacitive and memristive $I-V$ curve.

4. Conclusion

Thermal vacuum evaporation method was used to synthesize single-layer Sb_2Te_3 films and three-layer $Sb_2Te_3/Sb_2S_3/Sb_2Te_3$ structures. It is shown that conductivity of Sb_2Te_3 film has semiconductor behavior in the temperature range of 3−250 K and semimetallic behavior in the range of 250−350 K. Three-layer $Sb_2Te_3/Sb_2S_3/Sb_2Te_3$ structure has semiconductor behavior throughout the temperature range of 3−350 K, and its resistivity at room temperature is one order of magnitude greater than that of Sb_2Te_3 film. $Sb_2Te_3/Sb_2S_3/Sb_2Te_3$ structure has a high Seebeck coefficient which is, respectively, 1.5 and 3 times greater than Seebeck coefficient of film and single-crystal Sb_2Te_3, and thermoelectric power of Sb_2Te_3 and $Sb_2Te_3/Sb_2S_3/Sb_2Te_3$ is lower than that of single-crystal Sb_2Te_3. Sb_2Te_3 $I-V$ curve has memristive behavior with unipolar resistive switching observed in traditional

memristors, while $Sb_2Te_3/Sb_2S_3/Sb_2Te_3$ may be treated as a memristor model with parallel-connected capacitance.

Funding

The research was supported by the Russian-Armenian University by decree of the Ministry of Education and Science of the Russian Federation and Committee for Science of the Republic of Armenia as part of scientific project No. 21T-1C150.

Conflict of interest

The authors declare that they have no conflict of interest.

References

[1] Terry M. Tritt. Annu. Rev. Mater. Res., **41**, 433 (2011).
[2] H.J. Goldsmid. *Introduction to Thermoelectricity* (Springer Series in Mater. Sci., 2010) p. 60.
[3] S.V. Ovsyannikov, V.V. Shchennikov. Chem. Mater., **22**, 635 (2010).
[4] Doo Seok Jeong, Reji Thomas, R.S. Katiyar, J.F. Scott, H. Kohlstedt, A. Petraru, Cheol Seong Hwang. Rep. Progr. Phys., **75**, 076502 (2012).
[5] R.B. Jacobs-Gedrim, M.T. Murphy, F. Yang, N. Jain, M. Shanmugam, E. Sang Song, Y. Kandel, P. Hesamaddin, H. Yu Yu, M.P. Anantram, D.B. Janes, B. Yu. Appl. Phys. Lett., **112**, 133101 (2018).
[6] J.J. Zhang, N. Liu, H.J. Sun, P. Yan, Y. Li, S.J. Zhong, S. Xie, R.J. Li, X.S. Miao. J. Electron. Mater., **45**, 1154 (2016).
[7] Z. Lv, Y. Zhou, S.-T. Han, V.A.L. Roy. Materials Today, **21**, 537 (2018).
[8] C. Du, W. Ma, T. Chang, P. Sheridan, W.D. Lu. Adv. Funct. Mater., **25**, 4290 (2015).
[9] Y.V. Pershin, M. Di Ventra. Neural Netw., **23**, 881 (2010).
[10] B. Lv, S. Hu, W.Li, X.Di, L. Feng, J. Zhang, L. Wu, Y. Cai, B. Li, Zh. Lei. Int. J. Photoenergy, **2010**, Article ID 476589 (2010).
[11] Cheol-Min Park, Yoon Hwa, Nark-Eon Sung, Hun-Joon Sohn. J. Mater. Chem., **20**, 1097 (2010).
[12] M.A. Popescu. *Non-Crystalline Chalcogenicides* (Springer, Solid-State Science and *Technology Library, 2000). ISBN: 9780792366485.*
[13] Wenwen Zheng, Peng Bi, Haochen Kang, Wei Wei, Fengming Liu, Jing Shi, Luxi Peng, Ziyu Wang, Rui Xiong. Appl. Phys. Lett., **105**, 023901 (2014).
[14] G.J. Snyder, E.S. Toberer. Nature Mater., **7**, 105 (2008).
[15] Y.K. Kuo, K.M. Sivakumar, C.A. Su, C.N. Ku, S.T. Lin, A.B. Kaiser, J.B. Qiang, Q. Wang, C. Dong. Phys. Rev. B, **74**, 014208 (2006).
[16] V.V. Pryadun, D.V. Louzguine-Luzgin, L.V. Shvanskaya, A.N. Vasilieva. JETP Lett., **101**, 465 (2015).
[17] Y.R. Guo, F. Dong, C. Qiao, J.J. Wang, S.Y. Wang, Ming Xu, Y.X. Zheng, R.J. Zhang, L.Y. Chen, C.Z. Wang, K.M. Ho. Phys. Chem. Chem. Phys., **20**, 11768 (2018).
[18] A.A. Sherchenkov, S.A. Kozyukhin, P.I. Lazarenko, A.V. Babich, N.A. Bogoslovsky, I.V. Sagunova, E.N. Redichev. FTP, **51**, 154 (2017) (in Russian).
[19] Yu.V. Khrapovitskaya, N.E. Maslova, M.L. Zanaveskin. Nauka i obrazovanie: nauch. izd. MGTU im. N.E. Baumana, **12**, 329 (2013) (in Russian).
[20] B. Sun, Y. Chen, M. Xiao, G. Zhou, Sh. Ranjan, W. Hou, X. Zhu, Y. Zhao, S.A.T. Redfern, Y.N. Zhou. Nano Lett., **19**, 6461 (2019).
[21] B. Sun, M. Xiao, G. Zhou, Z. Ren, Y.N. Zhou, Y.A. Wu. Mater. Today Adv., **6**, 100056 (2020).